Nonlinear emergent elasticity and structural transitions of a skyrmion crystal under uniaxial distortion

Yangfan Hu,* Xiaoming Lan, and Biao Wang†
Sino-French Institute of Nuclear Engineering and Technology, Sun Yat-sen University, Zhuhai 519082, China

(Received 16 January 2019; revised manuscript received 20 May 2019; published 7 June 2019)

Emergent crystals are the periodic alignment of "emergent particles," i.e., localized collective behavior of atoms or their charges, spins, or orbits. The elasticity of these novel states of matter suffering mechanical loads can be strikingly softer than that of the underlying material, showing great strain-mediated tunability. However, the deformation and possible failure of emergent crystals under strong strain, vital for realizing related applications, are hitherto unclear. Here we theoretically study the nonlinear elasticity and structural transitions of a Skyrmion crystal (SkX) suffering uniaxial distortion. Under moderate tension, a SkX behaves like a ductile material, with an exotic negative crossover elastic stiffness and a negative emergent Poisson's ratio at appropriate conditions of magnetic field. Under strong strain, we observe at most six phase transitions, generating four novel emergent crystals that are thermodynamically metastable. We argue that this nondestructive polymorphism is a general feature for any emergent crystals exposed to mechanical loads.

DOI: 10.1103/PhysRevB.99.214412

I. INTRODUCTION

A recent outburst of interest in emergent crystals has occurred due to the discovery of skyrmions [1–4] and their "relatives" [5–7] with varying chirality [8,9], commensurability [10], and dimensionality [8,11]. Particularly, in bulk [8,12] and geometrically confined [13–15] magnetic materials, they appear to be localized spin textures with nontrivial topology. These topological objects behave as elementary particles in an emerging world, such that they form novel crystalline states at low temperature and melt under heating [16]. These emergent crystals benefit from the exotic local properties of their composing particles (e.g., mobility to electric current [17,18] and skyrmion Hall effects [19,20]), while giving rise to novel macroscopic emergent properties when interacting with external fields [21–23]. Systematic study of the deformation and instability of emergent crystals under different external fields provides a major challenge for us to understand these new states of matter and to develop reliable approaches toward precise manipulation.

Skyrmion crystals (SkXs) in chiral magnets are profoundly affected by deformation of the atomic crystal underneath. It is known that mechanical loads affect the stability [24–28] and the elementary excitations [29] of the SkXs. Moreover, a SkX inside an FeGe thin film is found to undergo significant deformation about 66 times larger than that of the underlying atomic lattice [23] when stretched, and this "emergent" elasticity of SkXs has also been observed in MnSi [23,30,31]. This exotic sensitivity of SkX deformation to the deformation of the underlying material provides a new approach of SkX manipulation and has been studied in the linear range [32,33]. Nevertheless, a key issue for application that remains unclear is the nonlinear and critical behavior of SkXs when subject to moderate or strong elastic fields.

*Corresponding author: huyf3@mail.sysu.edu.cn
†Corresponding author: wangbiao@mail.sysu.edu.cn

In this work, we study the nonlinear elasticity and structural phase transitions of Bloch-type SkXs suffering uniaxial distortion of the underlying material within an analytical framework [32,34]. The model used has proved its effectiveness by quantitatively reproducing for MnSi the phase diagram [8], the variation of elastic stiffness [35], and the changed stability of SkXs in thin films [36]. We find that a SkX in MnSi behaves like a typical ductile material under moderate uniaxial tension, but with an exotic negative emergent Poisson's ratio and an exotic negative crossover elastic stiffness at appropriate conditions. At strong tension, a SkX undergoes five or six subsequent structural phase transitions, leading to the appearance of four distorted SkX phases that are thermodynamically metastable. We find the exotic emergent elasticity of a SkX observed in an FeGe thin film suffering uniaxial tension [23] is caused by a triangle-square phase transition of the SkX.

II. RESULTS

A. Model

Consider a cubic helimagnet stabilized in the SkX phase suffering uniaxial distortion along the x axis; the equilibrium state of the system is determined by the following rescaled Helmholtz free-energy density functional [34]:

$$\begin{aligned}\widetilde{w}(\mathbf{m}) = \widetilde{w}_0 + \sum_{i=1}^{3}\left(\frac{\partial \mathbf{m}}{\partial r_i}\right)^2 + 2\mathbf{m}\cdot(\nabla\times\mathbf{m}) - 2\mathbf{b}\cdot\mathbf{m} \\ + t\mathbf{m}^2 + \mathbf{m}^4 + \sum_{i=1}^{3}\widetilde{A}_e\left(\frac{\partial m_i}{\partial r_i}\right)^2 + \varepsilon_{11}\big[\widetilde{K}\mathbf{m}^2 \\ + \widetilde{L}_1 m_1^2 + \widetilde{L}_2 m_3^2 + \widetilde{L}_{O1}(m_{1,2}m_3 - m_{1,3}m_2) \\ + \widetilde{L}_{O2}(m_{3,1}m_2 - m_{2,1}m_3) + \widetilde{L}_{O3}m_1(m_{2,3} - m_{3,2})\big],\end{aligned} \tag{1}$$

 ©2019 American Physical Society

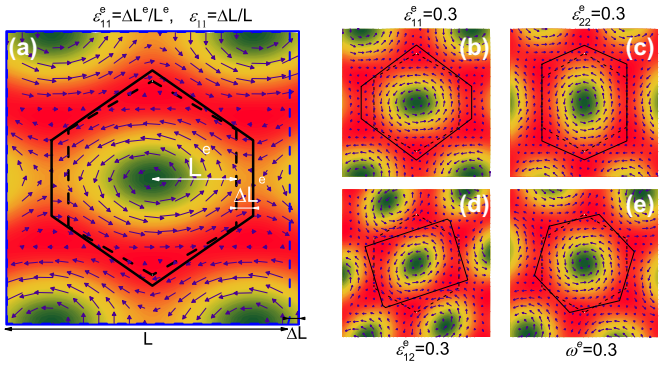

FIG. 1. Field configurations of deformed SkXs under various conditions. (a) A typical configuration of a SkX under uniaxial distortion, (b) $\varepsilon^e_{11} = 0.3$, (c) $\varepsilon^e_{22} = 0.3$, (d) $\varepsilon^e_{12} = 0.3$, and (e) $\omega^e = 0.3$. The vectors illustrate the distribution of the in-plane magnetization components with the length proportional to their magnitude, while the colored density plot illustrates the distribution of the out-of-plane magnetization component. The black dashed line plots the undeformed Wigner-Seitz cell, while the black solid line plots the deformed cell. The blue dashed line in (a) plots the undeformed material sample, while the blue solid line plots the deformed sample. (a) shows the physical meaning of ε_{11} and ε^e_{11}, in which case the only nonzero strain component is ε_{11} and the only nonzero emergent strain component is ε^e_{11}.

where $\mathbf{m}$ is the rescaled magnetization, ε_{11} is the strain component describing the uniaxial distortion, t is the rescaled temperature, $\mathbf{b}$ is the rescaled magnetic field, $\widetilde{A}_e$ is the rescaled exchange anisotropy coefficient, and $\widetilde{w}_0$ denotes the part of the free-energy density independent of the magnetization. To guarantee the validity of the results obtained, Eq. (1) contains a comprehensive description of magnetoelastic interaction derived based on group-theoretical analysis of B20 compounds [34], where the effects of strain can be categorized into three types [36]: (1) a renormalization of the coefficient of the second-order Landau expansion term by $\widetilde{K}$, (2) a uniaxial anisotropy determined by $\widetilde{L}_1$ and $\widetilde{L}_2$, and (3) an anisotropy of the Dzyaloshinskii-Moriya interaction (DMI) described by $\widetilde{L}_{O1}$, $\widetilde{L}_{O2}$, and $\widetilde{L}_{O3}$. The exchange anisotropy is considered in Eq. (1) since in previous studies it explains the intrinsic anisotropy as well as the direction-dependent stability of SkXs [37]. When the uniaxial distortion is applied along the y axis, Eq. (1) changes to Eq. (7) introduced in Sec. IV.

To describe the deformed SkXs, $\mathbf{m}$ is expanded within the nth-order Fourier expansion [32,38] as $\mathbf{m} = \mathbf{m}_0 + \sum_{i=1}^{n}\sum_{j=1}^{n_i} \mathbf{m}_{\mathbf{q}_{ij}} e^{i\mathbf{q}_{ij}(\varepsilon^e_{ij},\omega^e)\cdot\mathbf{r}}$, where $\mathbf{m}_0$ is a constant vector and $\mathbf{q}_{ij}(\varepsilon^e_{ij}, \omega^e)$ denotes the deformable reciprocal vectors whose deformation is described by the emergent elastic strains ε^e_{ij} and the emergent rotational angle ω^e (details shown in Sec. IV). Alternatively, we can write $\mathbf{m} = (\mathbf{m}^q, \boldsymbol{\varepsilon}^{ea})$, where the vector $\mathbf{m}^q$ contains all components of the vectors of Fourier magnitude $\mathbf{m}_0$ and $\mathbf{m}_{\mathbf{q}_{ij}}$ for all i and j and

$$\boldsymbol{\varepsilon}^{ea} = \left[\varepsilon^e_{11}, \varepsilon^e_{22}, \varepsilon^e_{12}, \omega^e\right]^T. \tag{2}$$

A remarkable feature of SkXs or any emergent crystals appearing in solid states is that two types of deformation coexist in the material considered, as illustrated in Fig. 1: deformation of the atomic lattice described by the strains ε_{ij} [Fig. 1(a)] and deformation of emergent crystals described by the emergent strains ε^e_{ij} and the emergent rotational angle ω^e [Fig. 1(b)].

At given values of t, $\mathbf{b}$, and ε_{11}, the equilibrium state of the SkX phase is determined by minimizing $\bar{w}(\mathbf{m}^q, \boldsymbol{\varepsilon}^{ea})$ with respect to all components of $\mathbf{m}^q$ and $\boldsymbol{\varepsilon}^{ea}$, where $\bar{w}(\mathbf{m}^q, \boldsymbol{\varepsilon}^{ea}) = \frac{1}{V}\int_V \widetilde{w}(\mathbf{m}^q, \boldsymbol{\varepsilon}^{ea})$ denotes the averaged free-energy density of the system. To guarantee that the solution obtained actually corresponds to a local minimum of the free energy of the system, the method of soft-mode analysis [38] is incorporated in the minimization process. A relation between ε_{11} and the equilibrium value of components of $\boldsymbol{\varepsilon}^{ea}$ characterizes the emergent elastic properties of SkXs under mechanical loads.

In addition to the free-energy minimization based on the Fourier representation introduced above, two other methods are also used to calculate the emergent elastic properties of SkXs under strain, namely, the Monte Carlo simulation and the theory of emergent elasticity. The Monte Carlo simulation also minimizes the Helmholtz free energy at given values of t, $\mathbf{b}$, and ε_{11}, but by discretizing Eq. (1) with two-dimensional (2D) grids in Cartesian coordinates instead of finding an analytical expression of $\mathbf{m}$ for SkXs. To use the theory of emergent elasticity, the emergent elastic strains of SkXs is calculated based on the assumption that $\boldsymbol{\varepsilon}^{ea}$ is linear to ε_{11}, where the linear coefficients are calculated at the equilibrium state of the SkX at given values of t, $\mathbf{b}$, and $\varepsilon_{11} = 0$. The details of the three methods used and a comparison between them are given in Sec. IV.

B. Elastic and nonlinear elastic behaviors of SkXs suffering moderate uniaxial tension of the underlying material

We study the elastic and nonlinear elastic behaviors of SkXs in MnSi (thermodynamic parameters are shown in Sec. IV) suffering moderate uniaxial tension of the underlying material. By "moderate" we mean the applied uniaxial tension does not induce a failure of the SkX phase, so that its deformation changes smoothly in the range of uniaxial tension considered. We analyze the variation of the components of $\boldsymbol{\varepsilon}^{ea}$ with ε_{11} calculated at different values of b and $\widetilde{A}_e$, where it is assumed that the SkX is distributed in the x-y plane and the rescaled magnetic field satisfies $\mathbf{b} = [0, 0, b]^T$.

We use three different methods to calculate the ε_{11}-$\boldsymbol{\varepsilon}^{ea}$ curves of SkXs at small strain, including the theory of emergent elasticity [32], the free-energy minimization based on fourth-order Fourier representation, and the Monte Carlo simulation method. As shown in Figs. 1(a) and 2(a), the results obtained by the three methods agree quantitatively well in the small-strain range and are exactly equal to each other when $\varepsilon_{11} \to 0$. At small strain, ε^e_{11} is almost linear with ε_{11} at all calculated conditions. The gradient of the ε_{11}-ε^e_{11} curve at $\varepsilon_{11} = 0$ is found to be sensitive to the value of applied magnetic field b. Specifically, the ε_{11}-ε^e_{11} curves calculated at $b = 0.3$ correspond to a negative gradient at $\varepsilon_{11} = 0$, indicating a compressed SkX along the x axis when the underlying material suffers elongation in the same direction. This result agrees with a previous study based on the theory of emergent elasticity [32], where the inverse of the gradient of the ε_{11}-ε^e_{11} curves at $\varepsilon_{11} = 0$ represents the component λ_{11} of the crossover strain ratio (CSR) matrix (introduced in Sec. IV).

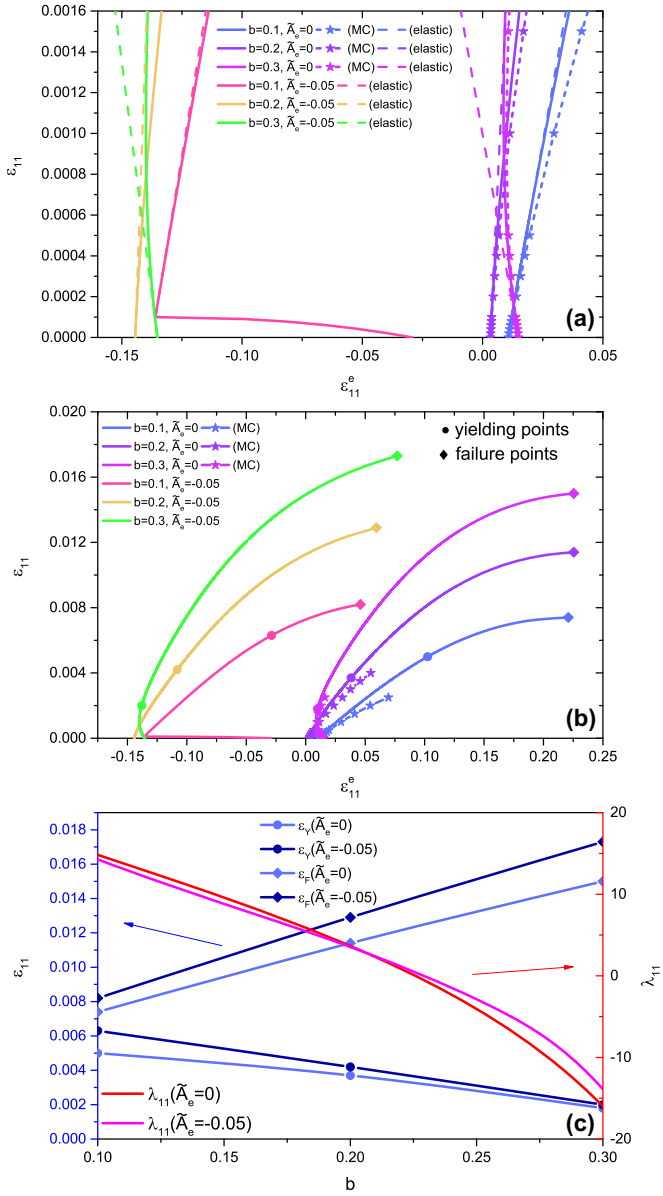

FIG. 2. Variation of ε^e_{11} with ε_{11} and related emergent elastic properties of SkXs in MnSi calculated at different values of b and $\widetilde{A}_e$. (a) ε_{11}-ε^e_{11} curves in the elastic stage, where solid curves are obtained through Fourier-representation-based free energy minimization, short-dashed curves with stars are obtained through Monte Carlo simulation, and long-dashed lines are obtained by calculating the CSR component λ_{11} under strain-free conditions. (b) ε_{11}-ε^e_{11} curves in the whole range of ε_{11} before failure, where circles mark the yield points and squares mark the failure points. (c) Variation of ε_Y and ε_F on the left axis and the strain-free CSR component λ_{11} on the right axis, with b.

In the wider range $0 \leqslant \varepsilon_{11} \leqslant 0.02$, the ε_{11}-ε^e_{11} curves [Fig. 2(b)] gradually show nonlinearity as ε_{11} increases. Specifically, at $b = 0.3$, the gradient of the ε_{11}-ε^e_{11} curve changes sign as ε_{11} increases, passing by a point ($\varepsilon_{11} \approx 0.001$) where it becomes singular. As shown in Fig. 3, uniaxial distortion of the material generally leads to complicated deformation of the SkX, especially when considering intrinsic anisotropic effects. When the material is stretched along the x axis, the SkX in the material deforms along the y axis, which is referred to as Poisson's effect for ordinary solids. As illustrated by the ε_{11}-ε^e_{22} curves in Fig. 3(a), SkXs possess a complicated Poisson's effect as ε_{11} increases. At $\widetilde{A}_e = -0.05$, ε^e_{12} and ω^e vary with ε_{11}, while at $\widetilde{A}_e = 0$ they vanish. Variation of ω^e with ε_{11} indicates that the SkX rotates globally when the material is stretched along the x axis. This is a type of deformation unseen in ordinary crystals.

C. Structural transitions of a skyrmion crystal in MnSi suffering uniaxial tension

When the applied uniaxial tension or compression is large enough, the SkX becomes intrinsically unstable, and structural phase transitions may occur. This has already been shown by the break points appearing near $\varepsilon_{11} = 0.0001$ in the $\varepsilon_{11} - \varepsilon^e_{11}$, $\varepsilon_{11} - \varepsilon^e_{12}$, and $\varepsilon_{11} - \omega^e$ curves at $b = 0.1$ in Figs. 2(a), 3(c) and 3(d).

We study the metastability and phase transitions of SkXs in MnSi at $t = 0.5$, $b = 0.3$ suffering uniaxial distortion and find that six types of nontrivial emergent crystalline states appear in MnSi suffering uniaxial tension. They are the triangle skyrmion crystal (T-SkX), rotated triangle skyrmion crystal (RT-SkX), deformed square skyrmion crystal (DS-SkX), elongated and rotated triangle skyrmion crystal (ERT-SkX), unstable skyrmion crystal (U-SkX), and in-plane single-Q (IPSQ) phase. The field configurations of these different phases are shown in the insets of Fig. 4. We choose ε^e_{11} and ω^e to be the order parameters of the system and plot their variation with ε_{11} in Fig. 4 to illustrate the behavior of different phases.

Interestingly, we find that immediately after the phase transition to the DS-SkX phase, the change of emergent elastic strain $\Delta\varepsilon^e_{11}$ compared with the strain-free SkX is about 60 times larger than the uniaxial strain ε_{11} applied to the underlying material. This result agrees quantitatively well with the significant deformation of the SkX observed in an FeGe thin film suffering uniaxial distortion [23]. Concerning the similarity of the crystalline structure between MnSi and FeGe, we argue that this phase transition from RT-SkX to DS-SkX explains the exotic emergent elasticity of SkX in FeGe.

Under uniaxial compression, the SkX quickly becomes unstable and evolves to the ferromagnetic state. This is predominantly explained by the renormalization of the coefficient of the second-order Landau expansion term due to the term $\varepsilon_{11}\widetilde{K}\mathbf{m}^2$ in Eq. (1) due to uniaxial compression, which leads to a decrease of the Curie temperature.

D. Effects of different terms in the magnetoelastic interaction on the phase transitions of a SkX

We have incorporated a comprehensive description of magnetoelastic interaction in the free-energy density functional given in Eq. (1). It will be useful to know the effects of different parts of the interaction and tell which is the dominant term. In Fig. 5, we present the results obtained with two different sets of magnetoelastic coupling parameters, where Fig. 5(a) is obtained by using the set of parameters of MnSi introduced in Sec. IV and Fig. 5(b) is obtained by setting $\widetilde{L}_{O1} = 0$, $\widetilde{L}_{O2} = 0$, $\widetilde{L}_{O3} = 0$ [i.e., Fig. 5(b) is obtained ignoring the DMI anisotropy induced by magnetoelastic coupling].

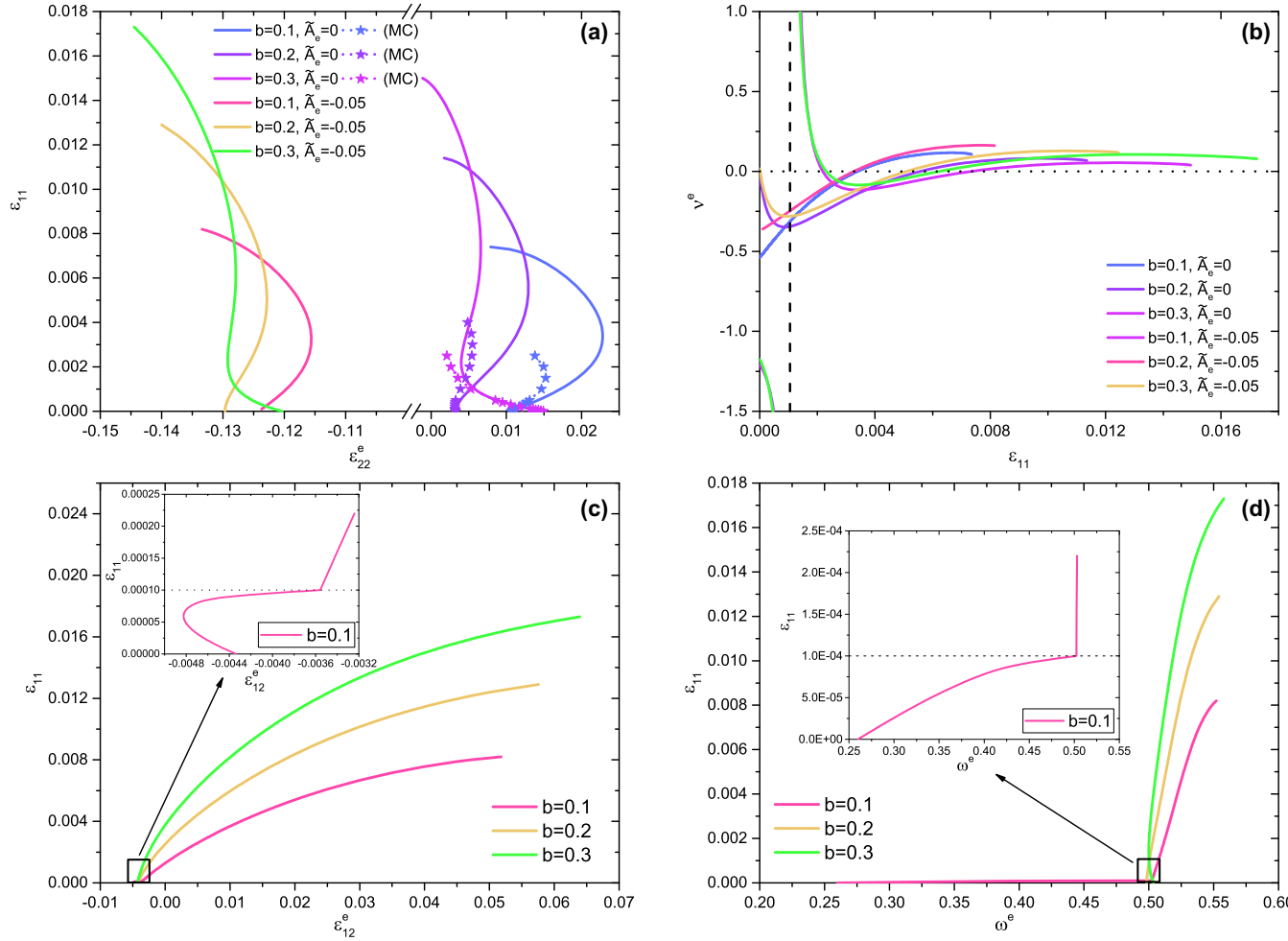

FIG. 3. Variation of other components of $\boldsymbol{\varepsilon}^{ea}$ with ε_{11} and related emergent elastic properties of SkXs in MnSi calculated at different values of rescaled magnetic field b and rescaled exchange anisotropy coefficient $\widetilde{A}_e$. (a) ε_{11}-ε^e_{22} curves, (b) ν^e-ε_{11} curves, (c) ε_{11}-ε^e_{12} curves, and (d) ε_{11}-ω^e curves calculated in the whole range of ε_{11} before failure. In (c) and (d), all the curves are plotted under the condition $\widetilde{A}_e = -0.05$, where the insets show break points at around $\varepsilon_{11} = 0.0001$ of the two curves calculated at $b = 0.1$.

The primary effect of this parameter change lies in the phase transition from DS-SkX to ERT-SkX changing from a second-order phase transition to a first-order phase transition in Fig. 5(b), while an intermediate phase, ERT_1-SkX, appears during this phase transition. Apart from this point, Fig. 5(b) is generally similar to Fig. 5(a). Since the $\widetilde{K}$ term in Eq. (5) describes the renormalization of the second-order Landau expansion term due to magnetoelastic coupling, it will not cause any anisotropy deformation of SkXs under any kind of mechanical load. In this case, our calculation shows that the terms with $\widetilde{L}_1$, $\widetilde{L}_2$, and $\widetilde{L}_3$ describing the uniaxial anisotropy due to magnetoelastic coupling dominate the behavior of SkXs in MnSi suffering uniaxial distortion, while the $\widetilde{L}_{Oi}$ ($i = 1, 2, \ldots, 6$) related terms describing the anisotropic DMI due to magnetoelastic coupling play a subsidiary role.

E. Strain-magnetic-field phase diagrams for MnSi

We further study the phase diagrams for MnSi suffering uniaxial distortion. We plot two types of ε_{11}-b phase diagrams under the conditions $t = 0.5$, $\widetilde{A}_e = -0.05$: the ε_{11}-b phase diagram of equilibrium states [Fig. 6(a)] and the ε_{11}-b phase diagram of metastability for the SkX [Fig. 6(b)]. It is found that a thermodynamically stable SkX exists in a very narrow range of ε_{11} and exists in only one state: the RT-SkX phase. On the other hand, concerning the robustness of the SkX [12,36], a metastable SkX exists in a much wider range of ε_{11} and is present in a variety of different phases.

Concerning the wave nature of emergent crystals [36], all metastable states are stabilized by nonlinear mode-mode interaction, while the corresponding thermodynamically stable state, the generalized-conical (G-conical) phase, is a single-Q structure whose wave vector is free to rotate in space. That is to say, the phase transition from any metastable emergent crystalline state to the G-conical phase is realized by the cancellation of all the nonlinear mode-mode interactions (i.e., setting all related Fourier amplitudes to zero). This is physically difficult because unlike annihilating a localized skyrmion, any Fourier component of magnetization exists globally and is hard to cancel through any local fluctuation. As a result, besides the well-known topological protection attributed to isolated skyrmions, the SkX is additionally protected globally by mode-mode interactions. In this sense, once we have a stable strain-free SkX phase, the appearance of various types

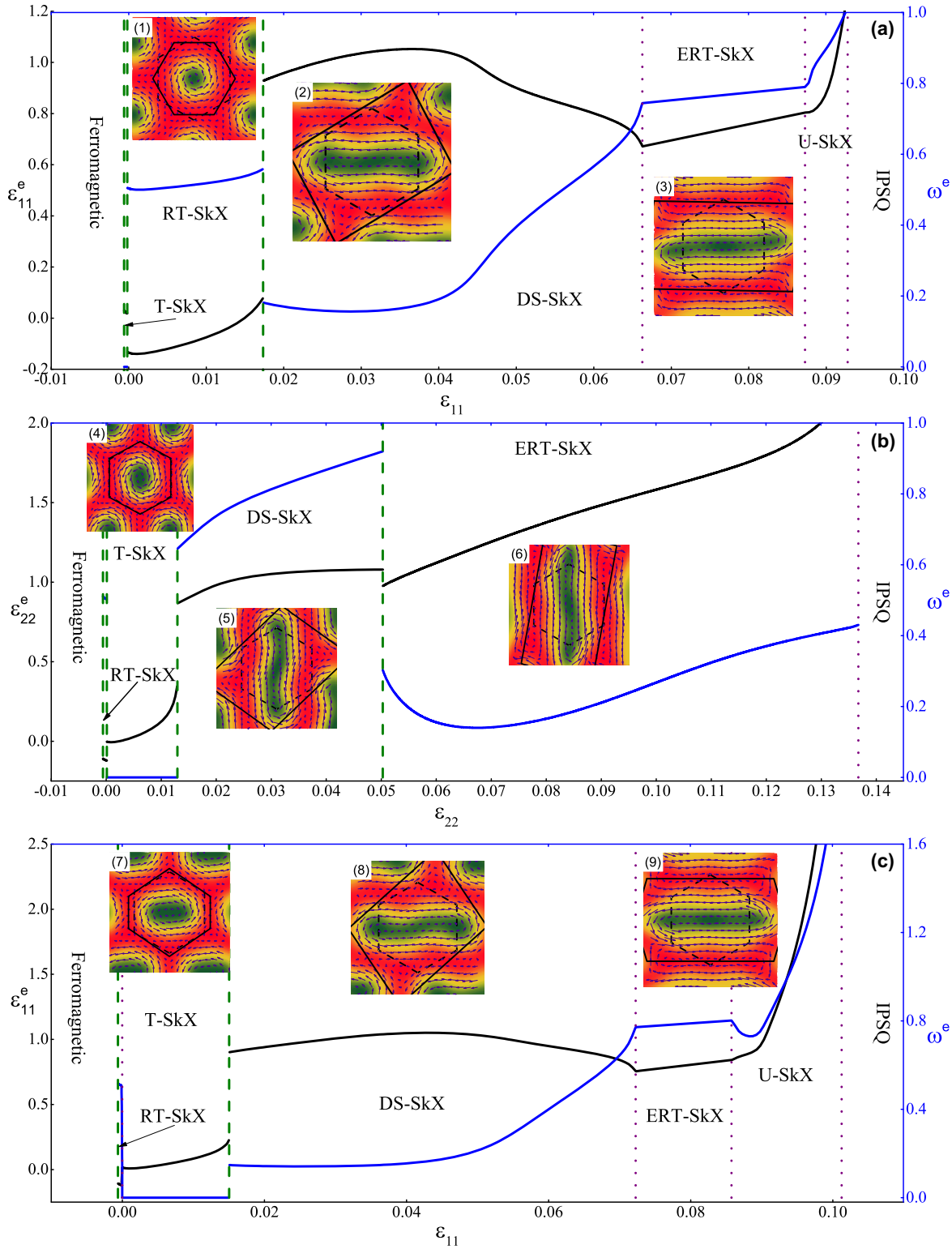

FIG. 4. Structural phase transitions of the SkX phase in MnSi suffering uniaxial distortion obtained at $t = 0.5$, $b = 0.3$. Different magnetic states appear as (a) and (c) ε_{11} and (b) ε_{22} increases, where (a) and (b) are calculated under the condition $\widetilde{A}_e = -0.05$ and (c) is calculated under the condition $\widetilde{A}_e = 0$. The existence of different phases is characterized by ε^e_{11} (on the left axis) and ω^e (on the right axis). The insets show the typical field configuration of magnetization for the corresponding phases, where the vectors illustrate the distribution of the in-plane magnetization components with length proportional to their magnitude, while the colored density plot illustrates the distribution of the out-of-plane magnetization component.

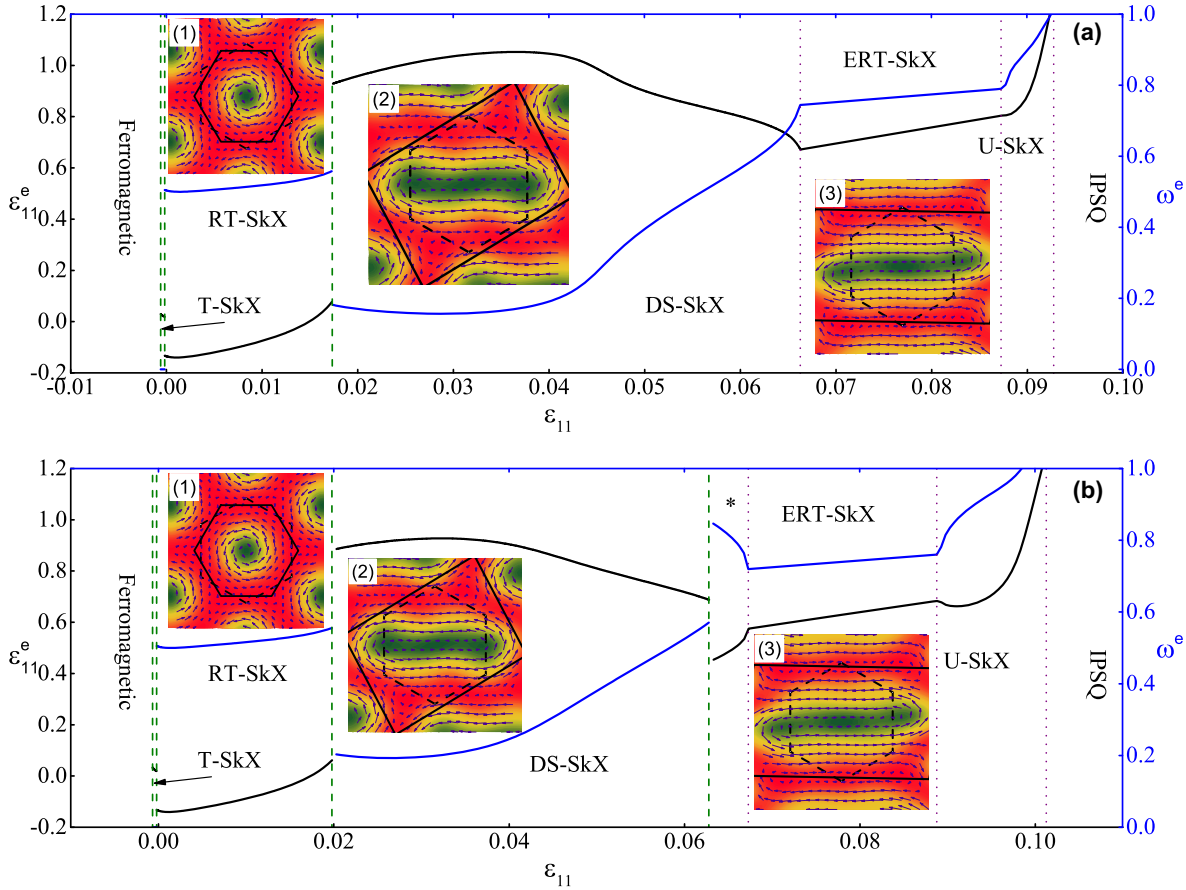

FIG. 5. Structural phase transitions of the SkX phase in MnSi suffering uniaxial distortion on the x axis obtained at $t = 0.5$, $b = 0.3$, $\widetilde{A}_e = -0.05$. (a) is plotted at $\widetilde{L}_{O1} = -0.38$, $\widetilde{L}_{O2} = 0.76$, $\widetilde{L}_{O3} = -0.38$, while (b) is plotted at $\widetilde{L}_{O1} = 0$, $\widetilde{L}_{O2} = 0$, $\widetilde{L}_{O3} = 0$. The existence of different phases is characterized by ε^e_{11} (on the left axis) and ω^e (on the right axis). The new phase appearing in (b) marked with and asterisk (*) is defined as the ERT_1-SkX phase.

of metastable SkXs predicted in our calculation is anticipated, especially in the low-temperature range. This viewpoint is supported by the successful observation of the DS-SkX phase in uniaxially stretched FeGe [23].

III. DISCUSSION

A. Nonlinear emergent elasticity of a skyrmion crystal in MnSi suffering uniaxial tension

In Fig. 2(b), the ε_{11}-ε^e_{11} curves correspond to the classic stress-strain curve of solid-state materials if one multiplies the y axis by Young's modulus of the material hosting the SkX. In this sense, the ε_{11}-ε^e_{11} curves characterizing the emergent elastic property of the SkX under uniaxial tension exhibit a shape similar to the stress-strain curve of any typical ductile metal (e.g., an aluminum alloy). As ε_{11} increases, the SkX "yields" before "failure," characterized by an emergent yielding strain ε_Y and an emergent failure strain ε_F. Imitating the definition of the yielding point for ductile materials such as an aluminum alloy, we define the emergent yielding point by the intersection of the ε_{11}-ε^e_{11} curve and the straight line determined by the strain-free λ_{11} right shifted by 2% on the ε^e_{11} axis. Different from atomic crystals, the yielding and failure of an emergent crystal describe, respectively, a nonlinear elastic behavior and a structural transition, which is recoverable after removing the applied strains. Similar to λ_{11}, ε_Y and ε_F are both sensitive to variation of the applied magnetic field, as illustrated in Fig. 2(c).

On the other hand, we define the emergent Poisson's ratio as $\nu^e = -\varepsilon^e_{22}/\varepsilon^e_{11}$ and plot in Fig. 3(b) the ν^e-ε_{11} curves calculated under various conditions. Under all calculated conditions, SkXs always possess a negative emergent Poisson's ratio in a considerable range of positive ε_{11}, which means the density of skyrmions in the SkX suffering mechanical forces is not conservative. This negative emergent Poisson's ratio of SkXs reminds one of auxetics, i.e., ordinary materials or structures with a negative Poisson's ratio. The similarity between the two is the presence of an internal structure in the unit cell. Nevertheless, the emergent elastic strains of the SkX are not work conjugates of the stresses. As a result, some deformation patterns that are forbidden in auxetics can occur in SkXs under external forces (e.g., at high b a SkX can shrink in the direction in which the underlying material is being stretched; such a deformation pattern cannot occur for auxetics).

B. Polymorphism and unlimited elasticity of magnetic emergent crystals

As shown in Fig. 4, under strong uniaxial distortion, the SkX possesses (a) polymorphism and (b) "unlimited

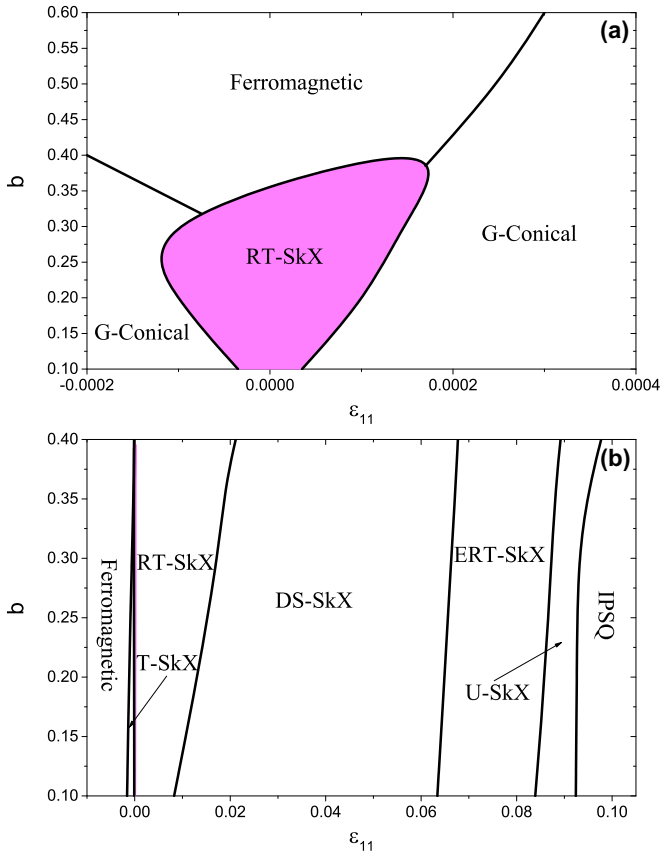

FIG. 6. ε_{11}-b phase diagrams of MnSi calculated at $\widetilde{A}_e = -0.05$. (a) ε_{11}-b phase diagram for the equilibrium states and (b) ε_{11}-b phase diagram for the metastable SkX phases.

elasticity" in the sense that the IPSQ phase can be regarded as a SkX with skyrmion particles infinitely stretched, and after removing the tension, the system recovers to its initial state. The many possible deformed SkX states appear mainly because of the complicated competition between the effects of uniaxial anisotropy and DMI anisotropy induced by uniaxial tension as described in Eq. (1). Since Eq. (1) is derived based on the symmetry requirement of B20 compounds, this exotic polymorphism under strain exists for any emergent crystals appearing in them. The unlimited elasticity of SkXs stems from a fundamental difference between atomic crystals and emergent crystals: the emergent deformation is realized by field configuration redistribution and is intrinsically nondestructive. We find that these two features dominate the nonlinear behavior of SkXs suffering all kinds of external fields, including not only mechanical loading but also magnetic field [39], electric field [20], and temperature field [40].

IV. METHODS

A. Thermodynamic potential for cubic helimagnets incorporating magnetoelastic interactions

To study the interaction between the elastic deformation of the material and the emergent elasticity of the skyrmion crystal, we consider the following rescaled free-energy density functional [34]:

$$\widetilde{w}(\mathbf{m}, \varepsilon_{ij}) = \sum_{i=1}^{3}\left(\frac{\partial \mathbf{m}}{\partial r_i}\right)^2 + \mathbf{m}\cdot(\nabla\times\mathbf{m}) - 2\mathbf{b}\cdot\mathbf{m} + t\mathbf{m}^2 + \mathbf{m}^4 + \sum_{i=1}^{3}\widetilde{A}_e\left(\frac{\partial m_i}{\partial r_i}\right)^2 + \widetilde{w}_{el} + \widetilde{w}_{me}, \tag{3}$$

where the first six terms on the right-hand side of Eq. (3) denote, respectively, the exchange energy density, the DMI, the Zeeman energy density, the second- and fourth-order Landau expansion terms, and the exchange anisotropy with a rescaled parameter $\widetilde{A}_e$ and

$$\widetilde{w}_{el} = \tfrac{1}{2}\widetilde{C}_{11}\left(\varepsilon_{11}^2+\varepsilon_{22}^2+\varepsilon_{33}^2\right) + \widetilde{C}_{12}\left(\varepsilon_{11}^2\varepsilon_{22}^2+\varepsilon_{22}^2\varepsilon_{33}^2+\varepsilon_{22}^2\varepsilon_{33}^2\right) + \tfrac{1}{2}\widetilde{C}_{44}\left(\gamma_{12}^2+\gamma_{13}^2+\gamma_{23}^2\right) \tag{4}$$

denotes the elastic energy density of materials with cubic symmetry, $\gamma_{ij} = 2\varepsilon_{ij}$ denote the engineering shear strains, and

$$\widetilde{w}_{me} = \widetilde{K}\mathbf{m}^2\varepsilon_{ii} + \widetilde{L}_1\left(m_1^2\varepsilon_{11}+m_2^2\varepsilon_{22}+m_3^2\varepsilon_{33}\right) + \widetilde{L}_2\left(m_3^2\varepsilon_{11}+m_1^2\varepsilon_{22}+m_2^2\varepsilon_{33}\right) + \widetilde{L}_3(m_1m_2\gamma_{12} + m_1m_3\gamma_{13}+m_2m_3\gamma_{23}) + \sum_{i=1}^{6}\widetilde{L}_{Oi}\widetilde{f}_{Oi} \tag{5}$$

denotes the magnetoelastic energy density, where

$$\begin{aligned}
\widetilde{f}_{O1} &= \varepsilon_{11}(m_{1,2}m_3 - m_{1,3}m_2) + \varepsilon_{22}(m_{2,3}m_1 - m_{2,1}m_3) + \varepsilon_{33}(m_{3,1}m_2 - m_{3,2}m_1),\\
\widetilde{f}_{O2} &= \varepsilon_{11}(m_{3,2}m_2 - m_{2,1}m_3) + \varepsilon_{22}(m_{1,2}m_3 - m_{3,2}m_1) + \varepsilon_{33}(m_{2,3}m_1 - m_{1,3}m_2),\\
\widetilde{f}_{O3} &= \varepsilon_{11}m_1(m_{2,3} - m_{3,2}) + \varepsilon_{22}m_2(m_{3,1} - m_{1,3}) + \varepsilon_{33}m_3(m_{1,2} - m_{2,1}),\\
\widetilde{f}_{O4} &= \gamma_{23}(m_{1,3}m_3 - m_{1,2}m_2) + \gamma_{13}(m_{2,1}m_1 - m_{2,3}m_3) + \gamma_{12}(m_{3,2}m_2 - m_{3,1}m_1),\\
\widetilde{f}_{O5} &= \gamma_{23}(m_{3,1}m_3 - m_{2,1}m_2) + \gamma_{13}(m_{1,2}m_1 - m_{3,2}m_3) + \gamma_{12}(m_{2,3}m_2 - m_{1,3}m_1),\\
\widetilde{f}_{O6} &= \gamma_{23}m_1(m_{3,3} - m_{2,2}) + \gamma_{13}m_2(m_{1,1} - m_{3,3}) + \gamma_{12}m_3(m_{2,2} - m_{1,1}),
\end{aligned} \tag{6}$$

with $m_{i,j} = \frac{\partial m_i}{\partial r_j}$. In Eq. (5), the magnetoelastic functional is derived for B20 helimagnets according to the symmetry requirement of point group T, where we have incorporated all necessary terms that matter. $\widetilde{K}$, $\widetilde{L}_1$, $\widetilde{L}_2$, $\widetilde{L}_3$, and $\widetilde{L}_{Oi}$ $(i = 1, 2, \ldots, 6)$ are thermodynamic parameters characterizing different orders of magnetoelastic interactions. To be more specific, the $\widetilde{K}$ term describes the renormalization of the second-order Landau expansion term due to magnetoelastic coupling, the terms with $\widetilde{L}_1$, $\widetilde{L}_2$, and $\widetilde{L}_3$ describe the uniaxial anisotropy due to magnetoelastic coupling, and the $\widetilde{L}_{Oi}$ $(i = 1, 2, \ldots, 6)$ related terms describe the anisotropic DMI due to magnetoelastic coupling. The thermodynamic parameters of MnSi used in the

calculation are presented in a rescaled form [34] as $\widetilde{C}_{11} = 1.51 \times 10^6$, $\widetilde{C}_{12} = 3.42 \times 10^5$, $\widetilde{C}_{44} = 6.28 \times 10^5$, $\widetilde{A}_e = -0.05$, $\widetilde{K} = -292.40$, $\widetilde{L}_1 = -10.24$, $\widetilde{L}_2 = 8.77$, $\widetilde{L}_3 = 12.03$, $\widetilde{L}_{O1} = -0.38$, $\widetilde{L}_{O2} = 0.76$, $\widetilde{L}_{O3} = -0.38$. The effectiveness of this set of parameters has been proved in explaining various types of magnetoelastic-related phenomena of SkXs [34]. To see the effect of a specific term during the calculation, we can intentionally set the corresponding parameters to zero and then see the changed outcomes (e.g., by comparing the results obtained at $\widetilde{A}_e = -0.05$ and $\widetilde{A}_e = 0$, we can see the effect of exchange anisotropy; by comparing the results obtained at $\widetilde{L}_{O1} = -0.38$, $\widetilde{L}_{O2} = 0.76$, $\widetilde{L}_{O3} = -0.38$ and $\widetilde{L}_{O1} = 0$, $\widetilde{L}_{O2} = 0$, $\widetilde{L}_{O3} = 0$, we can see the effect of magnetoelastic-coupling-induced DMI anisotropy). Equation (1) can be derived from Eq. (3) by setting all components of elastic strains to zero except ε_{11}. When the uniaxial distortion is applied along the axis y, by setting all components of elastic strains to zero except ε_{22}, we have from Eq. (3)

$$\begin{aligned}\widetilde{w}(\mathbf{m}) = \widetilde{w}_0 &+ \sum_{i=1}^{3}\left(\frac{\partial \mathbf{m}}{\partial r_i}\right)^2 + 2\mathbf{m}\cdot(\nabla\times\mathbf{m}) - 2\mathbf{b}\cdot\mathbf{m} \\ &+ t\mathbf{m}^2 + \mathbf{m}^4 + \sum_{i=1}^{3}\widetilde{A}_e\left(\frac{\partial m_i}{\partial r_i}\right)^2 + \varepsilon_{22}\big[\widetilde{K}\mathbf{m}^2 \\ &+ \widetilde{L}_1 m_2^2 + \widetilde{L}_2 m_1^2 + \widetilde{L}_{O1}(m_{2,3}m_1 - m_{2,1}m_3) \\ &+ \widetilde{L}_{O2}(m_{1,2}m_3 - m_{3,2}m_1) \\ &+ \widetilde{L}_{O3}m_2(m_{3,1} - m_{1,3})\big]. \end{aligned} \tag{7}$$

To determine a metastable emergent crystal in helimagnets, the rescaled magnetization $\mathbf{m}$ should be described mathematically as a Fourier series [38]:

$$\mathbf{m} = \mathbf{m}_0 + \sum_{i=1}^{\infty}\sum_{j=1}^{n_i}\mathbf{m}_{\mathbf{q}_{ij}} e^{i\mathbf{q}_{ij}(\boldsymbol{\varepsilon}^{ea})\cdot\mathbf{r}}. \tag{8}$$

It is convenient to expand $\mathbf{m}_{\mathbf{q}_{ij}}$ as $\mathbf{m}_{\mathbf{q}_{ij}} = \tilde{c}_{ij1}\mathbf{P}_{ij1} + \tilde{c}_{ij2}\mathbf{P}_{ij2} + \tilde{c}_{ij3}\mathbf{P}_{ij3}$, where $\tilde{c}_{ij1} = \tilde{c}^{re}_{ij1} + i\tilde{c}^{im}_{ij1}$, $\tilde{c}_{ij2} = \tilde{c}^{re}_{ij2} + i\tilde{c}^{im}_{ij2}$, $\tilde{c}_{ij3} = \tilde{c}^{re}_{ij3} + i\tilde{c}^{im}_{ij3}$ are complex variables to be determined and $\mathbf{P}_{ij1} = \frac{1}{\sqrt{2}s_i q}[-iq_{ijy}, iq_{ijx}, s_i q]^T$, $\mathbf{P}_{ij2} = \frac{1}{s_i q}[q_{ijx}, q_{ijy}, 0]^T$, $\mathbf{P}_{ij3} = \frac{1}{\sqrt{2}s_i q}[iq_{ijy}, -iq_{ijx}, s_i q]^T$, with $\mathbf{q}^0_{ij} = [q_{ijx}, q_{ijy}]^T$, $|\mathbf{q}^0_{ij}| = s_i q$. Assume that the undeformed wave vectors are $\mathbf{q}^0_{11} = q[0, 1]^T$, $\mathbf{q}^0_{12} = q[-\frac{\sqrt{3}}{2}, -\frac{1}{2}]^T$ for a hexagonal lattice; the deformed wave vectors are related to the emergent elastic strains and emergent rotation angle (in terms of the Green's strain tensor) by [32]

$$\begin{aligned}\mathbf{q}_{11} &= \frac{q}{s}\big[\omega^e - \varepsilon^e_{12}, 1 + \varepsilon^e_{11}\big]^T, \\ \mathbf{q}_{12} &= \frac{q}{2s}\big[-\sqrt{3} - \sqrt{3}\varepsilon^e_{22} + \varepsilon^e_{12} - \omega^e \\ &\quad - 1 - \varepsilon^e_{11} + \sqrt{3}\big(\varepsilon^e_{12} + \omega^e\big)\big]^T, \end{aligned} \tag{9}$$

where $s = 1 + \varepsilon^e_{11} + \varepsilon^e_{22} + \varepsilon^e_{11}\varepsilon^e_{22} - (\varepsilon^e_{12})^2 + (\omega^e)^2$. The averaged rescaled free-energy density for emergent crystalline states can be obtained by substituting Eqs. (8) and (9) into Eq. (3) and taking the volume average $\bar{w} = \frac{1}{V}\int \widetilde{w} dV$. The equilibrium state of any emergent crystal is determined through minimization of $\bar{w}$ with respect to $\boldsymbol{\varepsilon}^{ea}$, $\tilde{c}^{re}_{ijk}$, and $\tilde{c}^{im}_{ijk}$.

B. Emergent elasticity for 2D hexagonal emergent crystals in helimagnets

To formulate the theory of emergent elasticity [32] for emergent crystals in helimagnets, we first have to determine a metastable emergent crystal under the condition of interest. At small disturbance around this metastable state and neglecting possible periodic elastic fields, the averaged rescaled free-energy density for emergent crystalline states can be expanded in a quadratic form of all the independent variables as

$$\begin{aligned}\bar{w} = \bar{w}_u &+ \tfrac{1}{2}(d\boldsymbol{\varepsilon}^{ea})^T\widetilde{\mathbf{C}}^e d\boldsymbol{\varepsilon}^{ea} + \tfrac{1}{2}(d\mathbf{m}^q)^T\widetilde{\boldsymbol{\mu}}^q d\mathbf{m}^q \\ &+ \tfrac{1}{2}(d\boldsymbol{\varepsilon})^T\widetilde{\mathbf{C}}d\boldsymbol{\varepsilon} + (d\boldsymbol{\varepsilon})^T\widetilde{\mathbf{h}}d\boldsymbol{\varepsilon}^{ea} \\ &+ (d\boldsymbol{\varepsilon}^{ea})^T\widetilde{\mathbf{g}}^{eq}d\mathbf{m}^q + (d\boldsymbol{\varepsilon})^T\widetilde{\mathbf{g}}^q d\mathbf{m}^q, \end{aligned} \tag{10}$$

where quantities with the prefix d denote a small disturbance, $\bar{w}_u$ denotes the undisturbed averaged rescaled Helmholtz free-energy density, and

$$\boldsymbol{\varepsilon}^{ea} = \big[\varepsilon^e_{11}, \varepsilon^e_{22}, \varepsilon^e_{12}, \omega^e\big]^T, \tag{11}$$

$$\boldsymbol{\varepsilon} = [\varepsilon_{11}, \varepsilon_{22}, \varepsilon_{12}, \gamma_{23}, \gamma_{13}, \gamma_{12}]^T, \tag{12}$$

$$\begin{aligned}\mathbf{m}^q = \big[&m_{01}, m_{02}, m_{03}, \tilde{c}^{re}_{111}, \tilde{c}^{im}_{112}, \tilde{c}^{re}_{113}, \tilde{c}^{re}_{121}, \\ &\tilde{c}^{im}_{122}, \tilde{c}^{re}_{123}, \tilde{c}^{re}_{131}, \tilde{c}^{im}_{132}, \tilde{c}^{re}_{133}, \tilde{c}^{re}_{211}, \dots\big]^T, \end{aligned} \tag{13}$$

$$\begin{aligned}\widetilde{C}_{ij} &= \left(\frac{\partial^2\bar{w}}{\partial\varepsilon_i\partial\varepsilon_j}\right)_0, \quad \widetilde{h}_{ij} = \left(\frac{\partial^2\bar{w}}{\partial\varepsilon_i\partial\varepsilon^{ea}_j}\right)_0, \\ \widetilde{g}^q_{ij} &= \left(\frac{\partial^2\bar{w}}{\partial\varepsilon_i\partial m^q_j}\right)_0, \quad \widetilde{C}^e_{ij} = \left(\frac{\partial^2\bar{w}}{\partial\varepsilon^{ea}_i\partial\varepsilon^{ea}_j}\right)_0, \\ \widetilde{g}^{eq}_{ij} &= \left(\frac{\partial^2\bar{w}}{\partial\varepsilon^{ea}_i\partial m^q_j}\right)_0, \quad \widetilde{\mu}^q_{ij} = \left(\frac{\partial^2\bar{w}}{\partial m^q_i\partial m^q_j}\right)_0. \end{aligned} \tag{14}$$

One should notice that the form of Eq. (13) has been simplified after canceling the degrees of freedom related to the in-plane rigid translation [32]. The linear constitutive equations are derived from Eq. (10) as

$$\begin{aligned} d\boldsymbol{\sigma}^{ea} &= \widetilde{\mathbf{C}}^e d\boldsymbol{\varepsilon}^{ea} + \widetilde{\mathbf{h}}^T d\boldsymbol{\varepsilon} + \widetilde{\mathbf{g}}^{eq} d\mathbf{m}^q, \\ d\boldsymbol{\sigma} &= \widetilde{\mathbf{C}}d\boldsymbol{\varepsilon} + \widetilde{\mathbf{h}}d\boldsymbol{\varepsilon}^{ea} + \widetilde{\mathbf{g}}^q d\mathbf{m}^q, \\ d\mathbf{b}^q &= \boldsymbol{\mu}^q d\mathbf{m}^q + (\widetilde{\mathbf{g}}^q)^T d\boldsymbol{\varepsilon} + (\widetilde{\mathbf{g}}^{eq})^T d\boldsymbol{\varepsilon}^{ea}, \end{aligned} \tag{15}$$

where

$$\boldsymbol{\sigma}^{ea} = \big[\sigma^e_{11}, \sigma^e_{22}, \sigma^e_{12}, \Gamma^e_{12}\big]^T, \tag{16}$$

$$\boldsymbol{\sigma} = [\sigma_{11}, \sigma_{22}, \sigma_{33}, \sigma_{23}, \sigma_{13}, \sigma_{12}]^T, \tag{17}$$

$$\begin{aligned}\mathbf{b}^q = \big[&b_1, b_2, b_3, \tilde{d}^{re}_{111}, \tilde{d}^{im}_{112}, \tilde{d}^{re}_{113}, \tilde{d}^{re}_{121}, \\ &\tilde{d}^{im}_{122}, \tilde{d}^{re}_{123}, \tilde{d}^{re}_{131}, \tilde{d}^{im}_{132}, \tilde{d}^{re}_{133}, \tilde{d}^{re}_{211}, \dots\big]^T \end{aligned} \tag{18}$$

denote work conjugates of $\boldsymbol{\varepsilon}^{ea}$, $\boldsymbol{\varepsilon}$, and $\mathbf{m}^q$, respectively. When the material is subject to a disturbance of elastic strains, we

have $d\mathbf{b}^q = \mathbf{0}$ and $d\boldsymbol{\sigma}^{ea} = \mathbf{0}$. In this case, after deduction we have from Eq. (15)

$$d\boldsymbol{\varepsilon}^{ea} = \boldsymbol{\lambda} d\boldsymbol{\varepsilon}, \tag{19}$$

where

$$\begin{aligned} \boldsymbol{\lambda} &= -(\widetilde{\mathbf{C}}^{e*})^{-1}(\widetilde{\mathbf{h}}^{*})^T, \\ \widetilde{\mathbf{C}}^{e*} &= \widetilde{\mathbf{C}}^{e} - \widetilde{\mathbf{g}}^{eq}(\widetilde{\boldsymbol{\mu}}^{q})^{-1}(\widetilde{\mathbf{g}}^{eq})^T, \\ \widetilde{\mathbf{h}}^{e*} &= \widetilde{\mathbf{h}}^{e} - \widetilde{\mathbf{g}}^{q}(\widetilde{\boldsymbol{\mu}}^{q})^{-1}(\widetilde{\mathbf{g}}^{eq})^T. \end{aligned} \tag{20}$$

Equation (19) provides the linear relation between the emergent elastic strains, emergent rotations, and the elastic strains, and $\boldsymbol{\lambda}$ is called the crossover strain ratio matrix.

One should notice that the compliance matrices defined in Eq. (14) provide necessary information to determine the metastability of a magnetic phase. For a state obtained from free-energy minimization based on Fourier representation, the positive definiteness of the following matrix [38] guarantees the intrinsic stability of the state:

$$\boldsymbol{\Phi} = \begin{bmatrix} \widetilde{\mathbf{C}}^{e} & \widetilde{\mathbf{g}}^{eq} \\ (\widetilde{\mathbf{g}}^{eq})^T & \widetilde{\boldsymbol{\mu}}^{q} \end{bmatrix}. \tag{21}$$

When the positive definiteness of $\boldsymbol{\Phi}$ is destroyed, the eigenvector corresponding to the smallest eigenvalue (softest mode) of $\boldsymbol{\Phi}$ indicates the direction of evolution for the system from the current state.

C. Free-energy minimization based on Monte Carlo simulation

We perform Monte Carlo simulation based on an annealing algorithm to minimize the free energy of the system. To process the simulation, we discretize the free-energy density functional shown in Eq. (1) with 2D grids in Cartesian coordinates. Periodic boundary conditions are used in the calculation. For given elastic strains, the energy density functional can be written as

$$\widetilde{w} = \widetilde{w}(m_x(x, y), m_y(x, y), m_z(x, y)), \tag{22}$$

where m_x, m_y, m_z denote the components of the rescaled magnetization $\mathbf{m}$.

We use the central difference method to calculate the value of partial derivatives

$$\begin{aligned} \frac{\partial m_k}{\partial x}[i][j] &= \frac{m_k[i+1][j] - m_k[i-1][j]}{2\Delta x}, \\ \frac{\partial m_k}{\partial y}[i][j] &= \frac{m_k[i+1][j] - m_k[i-1][j]}{2\Delta y}, \\ k &= x, y, z, \end{aligned} \tag{23}$$

where the values of Δx and Δy determine the error of the Monte Carlo simulation.

In order to calculate the emergent strain of the SkX, Δx and Δy are also set as variables. In this case, we calculate the averaged free-energy density for different values of Δx and Δy to obtain the smallest one. And corresponding values of Δx and Δy determine the emergent elastic strains of the SkX,

$$\begin{aligned} \varepsilon^{e}_{11} &= \frac{\Delta x' - \Delta x}{\Delta x}, \\ \varepsilon^{e}_{22} &= \frac{\Delta y' - \Delta y}{\Delta y}. \end{aligned} \tag{24}$$

This method is applicable to only moderate emergent deformation of the SkX. When the difference between equilibrium values of Δx and Δy is too large, the precision can no longer be guaranteed, and a new set of grids is needed.

D. Comparison between different methods to calculate the emergent deformation of SkXs

We have introduced three different methods to study the emergent deformation of SkXs, including the theory of emergent elasticity (EE), the free-energy minimization based on fourth-order Fourier representation (MF), and the Monte Carlo simulation method (MC). In terms of the range of applicability, we have for the three methods MF, MC > EE. In principle, MF and MC can both be used to determine the emergent deformation of SkXs for any given condition of t, b, and ε_{ij}. Nevertheless, for MC, when there is emergent shearing and emergent rotation of the SkX, the shape of the calculated region and the periodic boundary condition both change, which is technically hard to deal with. In this work, we use MC only for the case where there is no emergent shearing and emergent rotation. EE, on the other hand, presumes a linear relation between the emergent elastic strains and the elastic strains. When such a linear assumption is no longer valid as ε_{ij} increases, the results obtained by EE are no longer reliable. In fact, the emergent yielding strain ε_Y defined and calculated in this work provides the upper limit where such an assumption is valid. In terms of the precision of results, we have for the three methods MF $\approx$ MC > EE. At given conditions of t, b, and ε_{ij}, the emergent deformation of the SkX determined by the two methods (MF and MC) through free-energy minimization can be as precise as one wants, where the precision of MF can be enhanced by increasing higher-order Fourier representation of the SkX and the precision of MC can be enhanced by increasing the size calculated and the density of the grids. The precision of results obtained by EE depends on the correctness of the linear assumption between the emergent elastic strains and the elastic strains. In terms of efficiency, we have for the three methods EE > MF > MC. When using EE, one calculates components of the linear compliance matrices at given t, b assuming a strain-free condition; then the emergent deformation of the SkX is determined by multiplying the corresponding compliance matrices by the given ε_{ij}. When using MF, the most time-consuming step is to derive the analytical expression of the free-energy functional in terms of the chosen order of Fourier representation of the SkX. Once this is obtained, the free-energy minimization can be performed at given conditions of t, b, and ε_{ij} with considerable speed, usually one order of magnitude faster than that of MC.

While all free-energy minimization has to be performed numerically, MF is intrinsically superior to MC as a solution method. The reason is that MF always yields an analytical expression of emergent crystals, while MC provides only

a discrete numerical distribution of the order parameters in space and/or time. Therefore, MF is recommended whenever it is suitable. Nevertheless, when there is a local field destroying the long-range order of magnetization, for which an analytical expression of **m** is no longer available, MC seems to be the only option.

ACKNOWLEDGMENTS

This work was supported by the National Natural Science Foundation of China (NSFC), Grants No. 11772360, 11832019, 11472313, and 11572355 and the Pearl River Nova Program of Guangzhou (Grant No. 201806010134).

[1] C. Bäuerle, Y. M. Bunkov, S. Fisher, H. Godfrin, and G. Pickett, Nature (London) **382**, 332 (1996).

[2] U. Al Khawaja and H. Stoof, Nature (London) **411**, 918 (2001).

[3] U. Rößler, A. Bogdanov, and C. Pfleiderer, Nature (London) **442**, 797 (2006).

[4] J. Fu, P. H. Penteado, M. O. Hachiya, D. Loss, and J. C. Egues, Phys. Rev. Lett. **117**, 226401 (2016).

[5] A. Nych, J.-i. Fukuda, U. Ognysta, S. Žumer, and I. Muševič, Nat. Phys. **13**, 1215 (2017).

[6] S. Huang, C. Zhou, G. Chen, H. Shen, A. K. Schmid, K. Liu, and Y. Wu, Phys. Rev. B **96**, 144412 (2017).

[7] P. J. Ackerman, J. Van De Lagemaat, and I. I. Smalyukh, Nat. Commun. **6**, 6012 (2015).

[8] S. Mühlbauer, B. Binz, F. Jonietz, C. Pfleiderer, A. Rosch, A. Neubauer, R. Georgii, and P. Böni, Science **323**, 915 (2009).

[9] I. Kézsmárki, S. Bordács, P. Milde, E. Neuber, L. Eng, J. White, H. M. Rønnow, C. Dewhurst, M. Mochizuki, K. Yanai *et al.*, Nat. Mater. **14**, 1116 (2015).

[10] M. C. Langner, S. Roy, S. K. Mishra, J. C. T. Lee, X. W. Shi, M. A. Hossain, Y.-D. Chuang, S. Seki, Y. Tokura, S. D. Kevan, and R. W. Schoenlein, Phys. Rev. Lett. **112**, 167202 (2014).

[11] T. Tanigaki, K. Shibata, N. Kanazawa, X. Yu, Y. Onose, H. S. Park, D. Shindo, and Y. Tokura, Nano Lett. **15**, 5438 (2015).

[12] K. Karube, J. White, N. Reynolds, J. Gavilano, H. Oike, A. Kikkawa, F. Kagawa, Y. Tokunaga, H. M. Rønnow, Y. Tokura *et al.*, Nat. Mater. **15**, 1237 (2016).

[13] X. Yu, Y. Onose, N. Kanazawa, J. Park, J. Han, Y. Matsui, N. Nagaosa, and Y. Tokura, Nature (London) **465**, 901 (2010).

[14] W. Jiang, G. Chen, K. Liu, J. Zang, S. G. te Velthuis, and A. Hoffmann, Phys. Rep. **704**, 1 (2017).

[15] H. Du, D. Liang, C. Jin, L. Kong, M. J. Stolt, W. Ning, J. Yang, Y. Xing, J. Wang, R. Che *et al.*, Nat. Commun. **6**, 7637 (2015).

[16] M. Ambrose and R. Stamps, New J. Phys. **15**, 053003 (2013).

[17] F. Jonietz, S. Mühlbauer, C. Pfleiderer, A. Neubauer, W. Münzer, A. Bauer, T. Adams, R. Georgii, P. Böni, R. A. Duine *et al.*, Science **330**, 1648 (2010).

[18] J. Zang, M. Mostovoy, J. H. Han, and N. Nagaosa, Phys. Rev. Lett. **107**, 136804 (2011).

[19] A. Neubauer, C. Pfleiderer, B. Binz, A. Rosch, R. Ritz, P. G. Niklowitz, and P. Böni, Phys. Rev. Lett. **102**, 186602 (2009).

[20] W. Jiang, X. Zhang, G. Yu, W. Zhang, X. Wang, M. B. Jungfleisch, J. E. Pearson, X. Cheng, O. Heinonen, K. L. Wang *et al.*, Nat. Phys. **13**, 162 (2017).

[21] Y. Shiomi, N. Kanazawa, K. Shibata, Y. Onose, and Y. Tokura, Phys. Rev. B **88**, 064409 (2013).

[22] J. S. White, K. Prša, P. Huang, A. A. Omrani, I. Živković, M. Bartkowiak, H. Berger, A. Magrez, J. L. Gavilano, G. Nagy, J. Zang, and H. M. Rønnow, Phys. Rev. Lett. **113**, 107203 (2014).

[23] K. Shibata, J. Iwasaki, N. Kanazawa, S. Aizawa, T. Tanigaki, M. Shirai, T. Nakajima, M. Kubota, M. Kawasaki, H. Park *et al.*, Nat. Nanotechnol. **10**, 589 (2015).

[24] Y. Nii, T. Nakajima, A. Kikkawa, Y. Yamasaki, K. Ohishi, J. Suzuki, Y. Taguchi, T. Arima, Y. Tokura, and Y. Iwasa, Nat. Commun. **6**, 8539 (2015).

[25] A. Chacon, A. Bauer, T. Adams, F. Rucker, G. Brandl, R. Georgii, M. Garst, and C. Pfleiderer, Phys. Rev. Lett. **115**, 267202 (2015).

[26] J. Wang, Y. Shi, and M. Kamlah, Phys. Rev. B **97**, 024429 (2018).

[27] E. Karhu, S. Kahwaji, T. L. Monchesky, C. Parsons, M. D. Robertson, and C. Maunders, Phys. Rev. B **82**, 184417 (2010).

[28] S. X. Huang and C. L. Chien, Phys. Rev. Lett. **108**, 267201 (2012).

[29] X.-X. Zhang and N. Nagaosa, New J. Phys. **19**, 043012 (2017).

[30] D. M. Fobes, Y. Luo, N. León-Brito, E. Bauer, V. Fanelli, M. Taylor, L. M. DeBeer-Schmitt, and M. Janoschek, Appl. Phys. Lett. **110**, 192409 (2017).

[31] S. Kang, H. Kwon, and C. Won, J. Appl. Phys. **121**, 203902 (2017).

[32] Y. Hu and B. Wang, arXiv:1608.04840.

[33] O. Petrova and O. Tchernyshyov, Phys. Rev. B **84**, 214433 (2011).

[34] Y. Hu and B. Wang, New J. Phys. **19**, 123002 (2017).

[35] Y. Nii, A. Kikkawa, Y. Taguchi, Y. Tokura, and Y. Iwasa, Phys. Rev. Lett. **113**, 267203 (2014).

[36] Y. Hu, Phys. Status Solidi RRL **12**, 1800247 (2018).

[37] X. Wan, Y. Hu, and B. Wang, Phys. Rev. B **98**, 174427 (2018).

[38] Y. Hu, Commun. Phys. **1**, 82 (2018).

[39] C. Wang, H. Du, X. Zhao, C. Jin, M. Tian, Y. Zhang, and R. Che, Nano Lett. **17**, 2921 (2017).

[40] D. Morikawa, X. Yu, K. Karube, Y. Tokunaga, Y. Taguchi, T.-h. Arima, and Y. Tokura, Nano Lett. **17**, 1637 (2017).